Available online at www.sciencedirect.com

SCIENCE DIRECT®

Vision Research 45 (2005) 3307–3321

Vision Research

www.elsevier.com/locate/visres

Initial ocular following in humans: A response to first-order motion energy

B.M. Sheliga *, K.J. Chen, E.J. FitzGibbon, F.A. Miles

Laboratory of Sensorimotor Research, National Eye Institute, National Institutes of Health, Building 49 Room 2A50, 49 Convent Drive, Bethesda, MD 20892, USA

Received 10 January 2005; received in revised form 18 March 2005

Abstract

Visual motion is sensed by low-level (energy-based) and high-level (feature-based) mechanisms. Ocular following responses (OFR) were elicited in humans by applying horizontal motion to vertical square-wave gratings lacking the fundamental (“missing fundamental stimulus”). Motion consisted of successive 1/4-wavelength steps, so the features and $4n + 1$ harmonics (where n = integer) shifted forwards, whereas the $4n - 1$ harmonics—including the strongest Fourier component (the 3rd harmonic)—shifted backwards (spatial aliasing). Initial OFR, recorded with the electromagnetic search coil technique, were always in the direction of the 3rd harmonic, e.g., leftward steps resulted in rightward OFR. Thus, the earliest OFR were strongly dependent on the motion of the major Fourier component, consistent with early spatio-temporal filtering prior to motion detection, as in the well-known energy model of motion analysis.
Published by Elsevier Ltd.

Keywords: Visual motion; Energy-based mechanisms; Missing fundamental; Spatio-temporal filtering

1. Introduction

It is generally held that there are two (or more) neural mechanisms by which we analyze visual motion. The distinguishing characteristics of these mechanisms are sometimes controversial, and various descriptors have been applied to them: “short-range” versus “long-range” (Braddick, 1974), “first-order” versus “second-order” (Cavanagh & Mather, 1989), “Fourier” versus “non-Fourier” (Chubb & Sperling, 1988), “passive” versus “active” (Cavanagh, 1992), and “energy-based” versus “feature-based” or “correspondence-based” (Smith, 1994).[1] Although these terms are based on data obtained using different approaches, there is a general consensus that the short-range/first-order/Fourier/passive/energy-based mechanism is low-level, utilizes dedicated local motion sensors, and functions without regard for form or perceptual features. Many computational models of this process have been suggested and, following up on the pioneering ideas of Reichardt (1961), the so-called motion-energy model has been particularly influential (Adelson & Bergen, 1985; van Santen & Sperling, 1985). Among the key features of this model are oriented spatio-temporal filters tuned for spatial frequency, which render it very sensitive to the Fourier composition of the luminance modulations in the motion stimulus. However, it is possible to design moving stimuli that are invisible to these low-level motion sensors—being defined not by luminance but by contrast, disparity or flicker, for example—and yet we have no problem seeing them move. Because of this, higher-level mechanisms have been proposed and these have been variously

* Corresponding author. Tel.: +1 301 402 4962; fax: +1 301 402 0511.
E-mail address: bms@lsr.nei.nih.gov (B.M. Sheliga).

[1] Lu and Sperling (1995, 1996, 2001) contend that there are three separate motion systems.

0042-6989/$ - see front matter. Published by Elsevier Ltd.
doi:10.1016/j.visres.2005.03.011

described, in accordance with some attribute of the preferred motion stimulus, as long-range/second-order/non-Fourier/active/feature-based/correspondence-based, but it is still not clear if these are sensed by one or more mechanisms: for recent review see Lu and Sperling (2001) and Derrington, Allen, and Delicato (2004).

There are some authors who argue that it is not necessary to invoke more than one sensing mechanism to account for our ability to see all the various kinds of motion. One of these proposals invokes gradient detectors that extract velocity by taking the ratio of the temporal and spatial derivatives of the luminance (Johnston & Clifford, 1995; Johnston, McOwan, & Buxton, 1992). However, Lu and Sperling (2001) argue that there is no clear theoretical basis for the recovery of second-order motion by gradient models, and they also find serious short-comings in other attempts to invoke a single mechanism to compute both first- and second-order motion (Grzywacz, Watamaniuk, & McKee, 1995; Taub, Victor, & Conte, 1997). A number of other authors have also cited evidence that they feel cannot be explained by a single mechanism (e.g., Derrington et al., 2004; Nishida, Ledgeway, & Edwards, 1997; Smith, 1994), but perhaps the most compelling case comes from data indicating that first- and second-order motion are sensed by different areas of the brain. Thus, recent studies using structural neuroimaging and psychophysics on patients with cortical lesions have reported a double dissociation in which one patient had a lesion that impaired his ability to sense first- but not second-order motion, and another patient with a lesion in a different region showed impairment in sensing second- but not first-order motion (Vaina & Cowey, 1996; Vaina, Cowey, & Kennedy, 1999; Vaina, Makris, Kennedy, & Cowey, 1998; Vaina & Soloviev, 2004).

Our interest is in the motion detectors underlying the initial ocular following responses (OFR) that can be elicited at ultra-short latency by sudden motion of a large textured pattern (Gellman, Carl, & Miles, 1990; Miles, Kawano, & Optican, 1986). On the one hand, initial OFR have the spatio-temporal properties expected of low-level motion detectors and show clear reversal with "first-order reverse-phi motion" (Masson, Yang, & Miles, 2002a), one of the hallmarks of an energy- or Fourier-based mechanism. On the other hand, in a study on one monkey, Benson and Guo (1999) reported that the initial OFR to motion defined by contrast-modulated static noise (pure second-order motion) were virtually identical to those recorded when the motion was defined by luminance modulations (first-order motion) except for a slightly longer latency (average difference, 10.8 ms). Masson and Castet (2002), working on humans, showed that unikinetic plaids consisting of two sine-wave gratings—one that is horizontal and moves vertically while the other is oblique (45°) and remains stationary—generated OFR with two components: initially, the responses were purely vertical (i.e., in the direction of the first-order Fourier motion), and then, after about 20 ms, the responses began to acquire a horizontal component (i.e., in the direction of the second-order pattern motion). Given these findings, it is surprising that Harris and Smith (1992), in a very careful study on humans, reported only very poor OKN in response to sustained, high-contrast, second-order motion stimuli (defined by contrast-modulated dynamic noise), though these same authors later showed that low-contrast second-order motion stimuli in the form of flicker-frequency-modulated noise were a little more effective and, when combined with first-order motion stimuli, modulated the OKN elicited by the latter (Harris & Smith, 2000). Higher-order stimuli in the form of disparity-defined motion (generated with dynamic random dots to eliminate monocular and first-order motion cues) have been shown to elicit vigorous OKN (Archer, Miller, & Helveston, 1987; Fox, Lehmkuhle, & Leguire, 1978), though the latency of these responses was not given, hence it is unclear if such stimuli generate OFR at the usual short latency for this response, which is <70 ms in monkeys (Miles et al., 1986) and <90 ms in humans (Gellman et al., 1990).

An important concern in these studies of the ocular tracking responses to large-field motion is that human subjects are known to be able to use attentive pursuit to track a variety of second-order motion stimuli (Butzer, Ilg, & Zanker, 1997; Hawken & Gegenfurtner, 2001; Lindner & Ilg, 2000). In the above-mentioned studies on OKN and OFR, various means were adopted to minimize the contribution of pursuit. These include, (1) the use of brief motion stimuli (in which the overall duration was <200 ms or, when more prolonged, comprised short-lived dynamic random dots), (2) the exclusion of images from the foveal region, and (3) instructing subjects to *not* track particular features. Such approaches are usually deemed successful if the associated saccades are in the opposite direction to the tracking eye movements (so-called quick phases) as though they were serving mainly to recenter the eyes without regard for any particular feature of the moving images (Fuchs, Reiner, & Pong, 1996). In contrast, when the associated saccades are in the same direction as the tracking (so-called catch-up saccades) it is generally assumed that they serve to foveate a particular moving feature and that the attentive pursuit mechanism has been deployed (Krauzlis, 2004).

In the present study we have recorded the initial OFR elicited at short latency by two kinds of apparent-motion stimuli whose features and principal Fourier components moved in opposite directions. Both were large, one-dimensional, vertical grating patterns that were shifted horizontally. The first will be referred to as the missing fundamental (or *mf*) stimulus, and can

be constructed from a square wave by subtracting the fundamental sine-wave component. When the *mf* stimulus moves smoothly it is perceived to move veridically. However, if it moves in discrete, 1/4-wavelength steps, then the direction of perceived motion is often reversed, i.e., opposite to its actual motion (Adelson, 1982; Adelson & Bergen, 1985; Baro & Levinson, 1988; Brown & He, 2000; Georgeson & Harris, 1990; Georgeson & Shackleton, 1989). The usual explanation for this is that first-order motion detectors are responsible for the perception here and do not sense the motion of the raw images (or their features) but rather a spatially filtered version of the images, so that the perceived motion depends critically on the Fourier composition of the spatial stimulus. In the frequency domain, a pure square wave is composed entirely of the odd harmonics (1st, 3rd, 5th, 7th etc.,) with progressively decreasing amplitudes such that the 3rd, 5th, 7th etc., have amplitudes that are 1/3rd, 1/5th, 1/7th etc., that of the 1st. Accordingly, the *mf* stimulus lacks the 1st harmonic and so is composed entirely of the higher odd harmonics, with the 3rd having the lowest spatial frequency and the largest amplitude. This means that when the *mf* stimulus shifts 1/4 of its (fundamental) wavelength, the largest Fourier component, the 3rd harmonic, shifts 3/4 of its own wavelength in the same (forward) direction. However, a 3/4-wavelength *forward* shift of a sine wave is exactly equivalent to a 1/4-wavelength *backward* shift and, because the brain gives greatest weight to the nearest image matches (spatial aliasing), the perceived motion is generally in the *backward* direction: see Fig. 1 (top). In fact, with 1/4-wavelength steps of the *mf* stimulus all of the $4n - 1$ harmonics (where n is an integer), such as the 3rd, 7th, 11th etc., shift 1/4 of their wavelength in the backward direction whereas all of the $4n + 1$ harmonics, such as the 5th, 9th, 13th etc., shift 1/4 of their wavelength in the forward direction, and it seems that the most prominent harmonic—the 3rd—generally dominates the perceived motion. It has been suggested (Georgeson & Shackleton, 1989) that this might be a form of motion capture (Ramachandran & Cavanagh, 1987), whereby the most salient spatial frequency component somehow suppresses the influence of all other components. For our present purposes, the important point is that the principal Fourier component and the features of the *mf* stimulus move in opposite directions.

The second apparent-motion stimulus that we have used, which was first introduced into the study of visual motion by Hammett, Ledgeway, and Smith (1993), will be referred to here as the *3f4f* stimulus and has the key properties of the *mf* stimulus but is somewhat simpler. This *3f4f* stimulus has a repeating pattern with a spatial frequency (or "beat") of f that is achieved by summing together two sinusoids of equal amplitude whose spatial frequencies are in the ratio 3:4 (the 3*f* and 4*f* components). When shifted forward in successive steps that are each 1/4 of the wavelength of the beat, the 4*f* component is effectively stationary while the 3*f* component, being stepped forward 3/4 of its wavelength, might be expected to show aliasing as though stepped backward 1/4 of its wavelength, exactly as with the *mf* stimulus: see Fig. 1 (bottom). In fact, motion transparency is generally reported with this stimulus, with rapid forward motion—presumed to be due to the motion of the pattern/feature—and slower reverse motion—presumed to be due to the motion of the 3*f* component—consistent with the simultaneous activation of feature-based and energy-based mechanisms, respectively (Hammett et al., 1993).

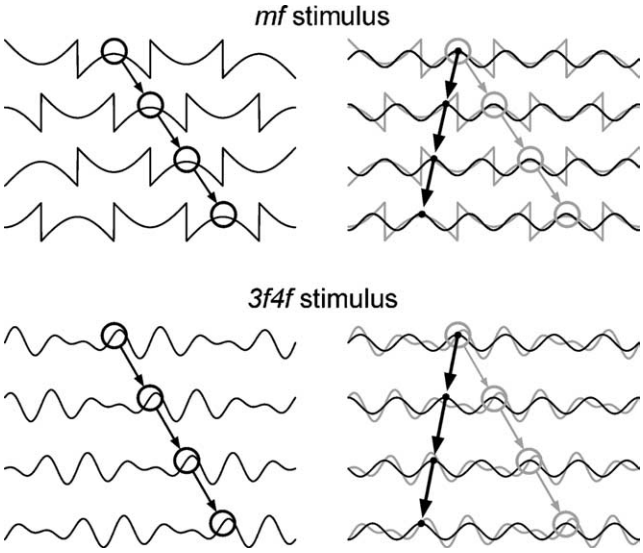

Fig. 1. The *mf* and *3f4f* stimuli. Traces show luminance as a function of horizontal spatial position when the stimuli undergo successive 1/4-wavelength *right*ward shifts. Top left: The *mf* stimulus; open circles and arrows indicate the *right*ward motion of one particular peak in the profile. Top right: The same *mf* stimulus (grey line) with superimposed 3rd harmonic (black line); open circles and arrows in grey indicate both the 1/4-wavelength *right*ward shifts of the overall pattern and the 3/4-wavelength *right*ward shifts of the 3rd harmonic; small filled circles and arrows in black indicate the 1/4-wavelength *left*ward shifts of the 3rd harmonic. Bottom left: The *3f4f* stimulus; open circles and arrows indicate the *right*ward motion of one particular feature of the profile. Bottom right: The same *3f4f* stimulus (grey line) with superimposed 3*f* component (black line); open circles and arrows in grey indicate both the 1/4-wavelength *right*ward shifts of the overall pattern and the 3/4-wavelength *right*ward shifts of the 3*f* component; small filled circles and arrows in black indicate the 1/4-wavelength *left*ward shifts of the 3*f* component.

We report that the initial OFR elicited by 1/4-wavelength steps applied to *mf* and *3f4f* gratings were invariably in the direction of the 3rd harmonic consistent with early spatio-temporal filtering and energy-based motion sensing. Two separate experiments are described, dealing with the dependence of these responses on spatial frequency and contrast, respectively, together with a number of critical controls.

2. Experiment 1: Dependence of initial OFR on spatial frequency

This first experiment concentrated on the general form of the initial OFR to *mf* and 3*f*4*f* apparent-motion stimuli and their quantitative dependence on spatial frequency.

2.1. Methods

Some of the techniques, such as those used for recording eye movements and for data analysis, were very similar to those used previously in our laboratory (Masson, Busettini, Yang, & Miles, 2001; Masson, Yang, & Miles, 2002b; Yang & Miles, 2003) and, therefore, will only be described in brief here. Experimental protocols were approved by the Institutional Review Committee concerned with the use of human subjects.

2.1.1. Subjects

Three subjects participated; two were authors (FAM, BMS) and the third was a paid volunteer who was unaware of the purpose of the experiments (JKM). All had normal or corrected-to-normal vision. Viewing was binocular for FAM and BMS, and monocular for JKM (right eye viewing).

2.1.2. Visual display and the grating stimuli

The subjects sat in a dark room with their heads positioned by means of adjustable rests for the forehead and chin, and held in place with a head band. Visual stimuli were presented on a computer monitor (Silicon Graphics CPD G520K 19'' CRT driven by a PC Radeon 9800 Pro video card) located straight ahead at 45.7 cm from the corneal vertex. The monitor screen was 385 mm wide and 241 mm high, with a resolution of 1920×1200 pixels and a vertical refresh rate of 100 Hz. The RGB signals from the video card provided the inputs to an attenuator (Pelli & Zhang, 1991) whose output was connected to the ''green'' input of a video signal splitter (Black Box Corp., AC085A-R2); the three ''green'' video outputs of the splitter were then connected to the RGB inputs of the monitor. This arrangement allowed the presentation of black and white images with 11-bit grayscale resolution. Initially, a luminance look-up table with 64 equally-spaced luminance levels ranging from 0.5 to 84.7 cd/m^2 was created by direct luminance measurements (IL1700 photometer; International Light Inc., Newburyport, MA) under software control. This table was then expanded to 2048 equally-spaced levels by interpolation and subsequently checked for linearity (typically, $r > 0.99998$).

The visual images consisted of one-dimensional vertical grating patterns that could have one of three horizontal luminance profiles in any given trial: (1) a pure sine wave, (2) a square wave with a missing fundamental (*mf* stimulus), (3) a sum of two equal-amplitude sinusoids whose spatial frequencies were in the ratio 3:4 (*3f4f* stimulus). Each image extended 257 mm horizontally (31.4°; 1280 pixels) and 206 mm vertically (25.4°; 1024 pixels) and had a mean luminance of 42.6 cd/m^2. This image was surrounded by a uniform gray border (with this same luminance) that extended out to the boundaries of the screen. The initial phase of a given grating was randomized from trial to trial at intervals of 1/4-wavelength. Motion was created by substituting a new image every frame (i.e., every 10 ms) for a total of 20 frames (i.e., stimulus duration, 200 ms), each new image being identical to the previous one except phase shifted horizontally by 1/4 of the wavelength of the fundamental. In any given trial the successive steps were all in the same direction (rightward or leftward, randomly selected). The dependent variable in this first experiment was the spatial frequency of the grating, randomly sampled each trial from a lookup table. For the pure sine-wave stimuli, the entries in the table were: 0.0417, 0.0625, 0.125, 0.25, 0.5, 1, 2, and 5 cycles/°. The entries for the *mf* and *3f4f* stimuli, indicating the spatial frequency of the overall pattern, were the same except that the highest spatial frequency (5 cycles/°) was omitted. The Michelson contrast, defined as $((L_{max} - L_{min})/(L_{max} + L_{min})) * 100\%$, where L is the luminance, was 32% for the pure sinusoids and for the 3*f* components of the *mf* stimuli as well as for the 3*f* and 4*f* components of the *3f4f* stimuli.

The display had a resolution of 40 pixels/° at the center, so that any components of the stimuli with spatial frequencies above 20 cycles/° (the Nyquist Frequency) would be aliased to lower frequencies. Thus, if a broadband stimulus like the *mf* were produced by merely subtracting the fundamental from the square wave then the resulting image might have significant energy at frequencies above the Nyquist Frequency, resulting in an aliasing problem. The amplitude of the *i*th harmonic in a *mf* grating is proportional to 1/*i*, i.e., the higher the harmonic the smaller its amplitude, so that as the spatial frequency of the *mf* grating is increased the Nyquist limit of the display is reached at progressively lower harmonics that have progressively higher contrast. Thus, aliasing problems increase as the spatial frequency of the *mf* grating increases. To avoid spatial aliasing, the *mf* stimuli were synthesized by summing the odd harmonics and including only those with spatial frequencies below the Nyquist Frequency. Thus, the 2 cycles/° *mf* grating was produced by summing the 3rd through the 9th odd harmonics so that the highest spatial frequency was 18 cycles/° and its contrast was 10.8%. Similarly, the 1 cycle/° *mf* grating was rendered up to the 19th harmonic (19 cycles/°; contrast, 5.1%), the 0.5 cycles/° *mf* grating up to the 39th harmonic (19.5 cycles/°; contrast, 2.5%), the 0.25 cycles/° *mf* grating up to the 79th harmonic

(19.75 cycles/°; contrast, 1.2%), the 0.125 cycles/° *mf* grating up to the 159th harmonic (19.88 cycles/°; contrast, 0.6%), the 0.0625 cycles/° *mf* grating up to the 319th harmonic (19.94 cycles/°; contrast, 0.3%), and the 0.0417 cycles/° *mf* grating up to the 479th harmonic (19.96 cycles/°; contrast, 0.2%). Note that all spatial frequencies given in this paper refer to the maximum seen value, which is the value at that point on the screen directly ahead of each eye, and, because the images were on a tangent screen, the spatial frequency seen by the subject increased with eccentricity from that point.

We shall refer to OFR that were in the same direction as the 1/4-wavelength shift of the whole grating as in the *forward* direction, and OFR in the opposite direction as in the *backward* direction. With the *mf* stimuli, the motion of the features and of the $4n + 1$ harmonics (of which the most powerful was the 5th) was in the forward direction, whereas the motion of the $4n - 1$ harmonics (of which the most powerful was the 3rd) was in the backward direction. With the *3f4f* stimuli, the motion of the features was in the forward direction whereas the motion of the 3*f* component was in the backward direction and the 4*f* component was stationary. Of course, with pure sine waves, there was only one Fourier component and this always moved in the same direction as the "feature".

2.1.3. Eye-movement recording

The horizontal and vertical positions of the right eye were recorded with an electromagnetic induction technique (Robinson, 1963) using a scleral search coil embedded in a silastin ring (Collewijn, Van Der Mark, & Jansen, 1975), as described by Yang, FitzGibbon, and Miles (2003).

2.1.4. Procedures

All aspects of the experimental paradigms were controlled by two PCs, which communicated via Ethernet using the TCP/IP protocol. One of the PCs was running a Real-time EXperimentation software package (REX) developed by Hays, Richmond, and Optican (1982), and provided the overall control of the experimental protocol as well as acquiring, displaying, and storing the eye-movement data. The other PC was running Matlab subroutines, utilizing the Psychophysics Toolbox extensions (Brainard, 1997; Pelli, 1997), and generated the visual stimuli upon receiving a start signal from the REX machine.

At the beginning of each trial, a grating pattern appeared (randomly selected from a lookup table) together with a central target spot (diameter, 0.25°) that the subject was instructed to fixate. After the subject's right eye had been positioned within 2° of the fixation target and no saccades had been detected (using an eye velocity threshold of 12°/s) for a randomized period of 600–900 ms the fixation target disappeared and the apparent-motion stimulus began. The motion lasted for 200 ms, at which point the screen became a uniform gray (luminance, 42.6 cd/m^2) marking the end of the trial. After an inter-trial interval of 500 ms a new grating pattern appeared together with a fixation point, commencing a new trial. The subjects were asked to refrain from blinking or making any saccades except during the inter-trial intervals but were given no instructions relating to the motion stimuli. If no saccades were detected during the period of the trial, then the data were stored on a hard disk; otherwise, the trial was aborted and subsequently repeated. Each block of trials had 44 randomly interleaved stimulus combinations: 3 grating patterns, each with 7 or 8 spatial frequencies (indicated above), and 2 directions of motion. Data were collected over several sessions until each condition had been repeated an adequate number of times to permit good resolution of the responses (through averaging) even when exploring the limit of the responsive range with stimuli of marginal efficacy; the actual numbers of trials will be given in the Results.

2.1.5. Data analysis

The horizontal and vertical eye position data obtained during the calibration procedure were each fitted with third-order polynomials which were then used to linearize the horizontal and vertical eye position data recorded during the experiment proper. Rightward eye movements were defined as positive. The eye-position data were smoothed with a 6-pole Butterworth filter (3 dB at 60 Hz), and velocity traces were derived from the two-point (20 ms apart) central difference between the symmetric-weight moving averages (7 points) of the position samples (Usui & Amidror, 1982). Trials with saccadic intrusions were deleted. Mean temporal profiles (position and velocity) were computed for each subject for all the data obtained for each of the 44 stimulus conditions. The initial horizontal OFR were quantified by measuring the changes in horizontal eye position over the 90-ms time periods commencing 60 ms after the onset of the motion stimuli. The minimum latency of onset was ~75 ms so that these response measures were restricted to the period prior to the closure of the visual feedback loop (i.e., twice the reaction time): initial open-loop responses. We then computed the means of these change-in-eye-position measures for each subject for each stimulus condition. The responses to rightward and leftward were pooled to improve the signal-to-noise by subtracting the mean response to each leftward motion stimulus from the mean response to the corresponding rightward motion stimulus, and we shall refer to these as "the R–L response measures". As rightward eye movements were positive in our sign convention, these pooled measures were positive when OFR were in the forward direction.

2.2. Results

2.2.1. Main experiment

The initial OFR elicited by successive 1/4-wavelength shifts applied to *mf* and *3f4f* stimuli were invariably in the direction of the 3rd harmonic, i.e., in the *backward* direction, whereas the OFR elicited when such shifts were applied to pure sinusoids were always in the *forward* direction. This can be seen in Fig. 2, which shows sample mean eye velocity profiles over time obtained from one subject with each of the three types of gratings using three different spatial frequencies (values in cycles/° indicated by the numbers at the end of the traces). In this figure, the OFR elicited by *left*ward shifts are shown in the upper row and the OFR elicited by *right*ward shifts are shown in the lower row. Since upward deflections of the traces denote rightward eye movement, it is evident that when the 1/4-wavelength shifts were *left*ward the resulting OFR were *right*ward with the *mf* and *3f4f* stimuli and *left*ward with the sine-wave stimuli: see Fig. 2(A)–(C). Everything was reversed with *right*ward shifts: see Fig. 2(D)–(F).

The quantitative dependence on spatial frequency, based on the mean R–L response measures, was quite similar in all 3 subjects. This is evident from the spatial frequency tuning curves plotted in Fig. 3, the data for individual subjects being shown in A, B, and C, and the normalized average data for all subjects in D. With the pure sine-wave stimuli (open circles in Fig. 3), the mean R–L response measures were all positive (OFR in the forward direction) and displayed a bandpass dependence on log spatial frequency that was well captured by Gaussian functions (r^2 values: 0.984, 0.995, and 0.987) with peaks (f_0) at 0.26, 0.24, and 0.24 cycles/° and standard deviations (σ) of 1.16, 1.18, and 1.16 natural log units: see the continuous smooth curves in Fig. 3. These parameters of the fitted Gaussian functions were used to derive a low-frequency cutoff (f_{lo}) and a high-frequency cutoff (f_{hi}), defined as the spatial frequencies at which the tuning curve was half its maximum, using the following expression from Read and Cumming (2003): $f_0 \exp(\pm\sigma\sqrt{\ln 4})$. The computed values of f_{lo} were 0.07, 0.06, and 0.06 cycles/°, and the computed values of f_{hi} were 1.03, 0.97, and 0.96 cycles/°. The parameters of the best-fit Gaussian for the normalized average data in Fig. 3(D) ($r^2 = 0.995$) were as follows: $f_0 = 0.25$ cycles/°, $\sigma = 1.17$ natural log units, $f_{lo} = 0.06$ cycles/°, and $f_{hi} = 0.99$ cycles/°.

With the *3f4f* stimuli, the mean R–L response measures were all negative (OFR in the backward direction) and their spatial frequency tuning curves (closed diamonds and dashed black lines in Fig. 3) were shifted to the left of those for the pure sine-wave data. Such a shift would be expected if the response were driven mainly by the motion of the 3*f* component rather than the motion of the overall pattern. If the responses to the *3f4f* gratings were *solely* determined by their 3*f* component then, when replotted as a function of the frequency of that 3*f* component, the *3f4f* data should show the same dependence on spatial frequency as the pure sine-wave data. When so replotted—with a sign inversion to facilitate easy comparison—the *3f4f* data usually fell slightly short of the pure sine-wave data: see the gray dashed lines in Fig. 3 and the vertical hatching in Fig. 3(D). The mean R–L responses to the *mf* stimuli were also all in the backward direction and roughly comparable with those obtained with the *3f4f* stimuli at the higher spatial frequencies but invariably fell short of them at lower spatial frequencies: see the open squares and linking straight lines in Fig. 3. When

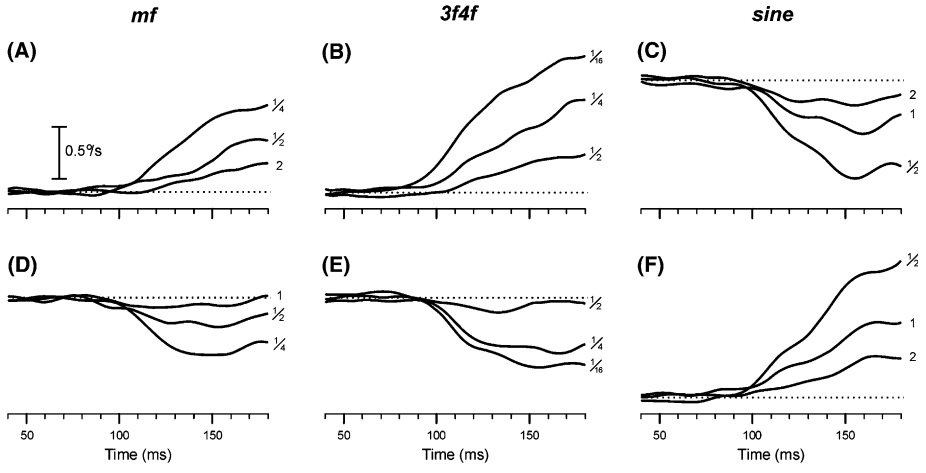

Fig. 2. The initial OFR: dependence on spatial frequency (eye velocity traces). Traces show the horizontal OFR resulting from successive leftward (upper row) and rightward (lower row) 1/4-wavelength steps applied to various types of gratings (subject, JKM). A and D: *mf* stimulus. B and E: *3f4f* stimulus. C and F: pure sine-wave stimulus. Each trace is the mean eye velocity response to 171–195 repetitions of the stimulus. Note that time on the abscissa starts 40 ms after the occurrence of the first step. The numbers at the ends of the traces indicate the fundamental spatial frequencies of the patterns in cycles/°. Upward deflections of the traces denote rightward eye movements, the dotted lines indicating zero eye velocity. Contrast was 32% for the pure sinusoids and for the 3*f* components of the *mf* stimuli as well as for the *3f* and *4f* components of the *3f4f* stimuli.

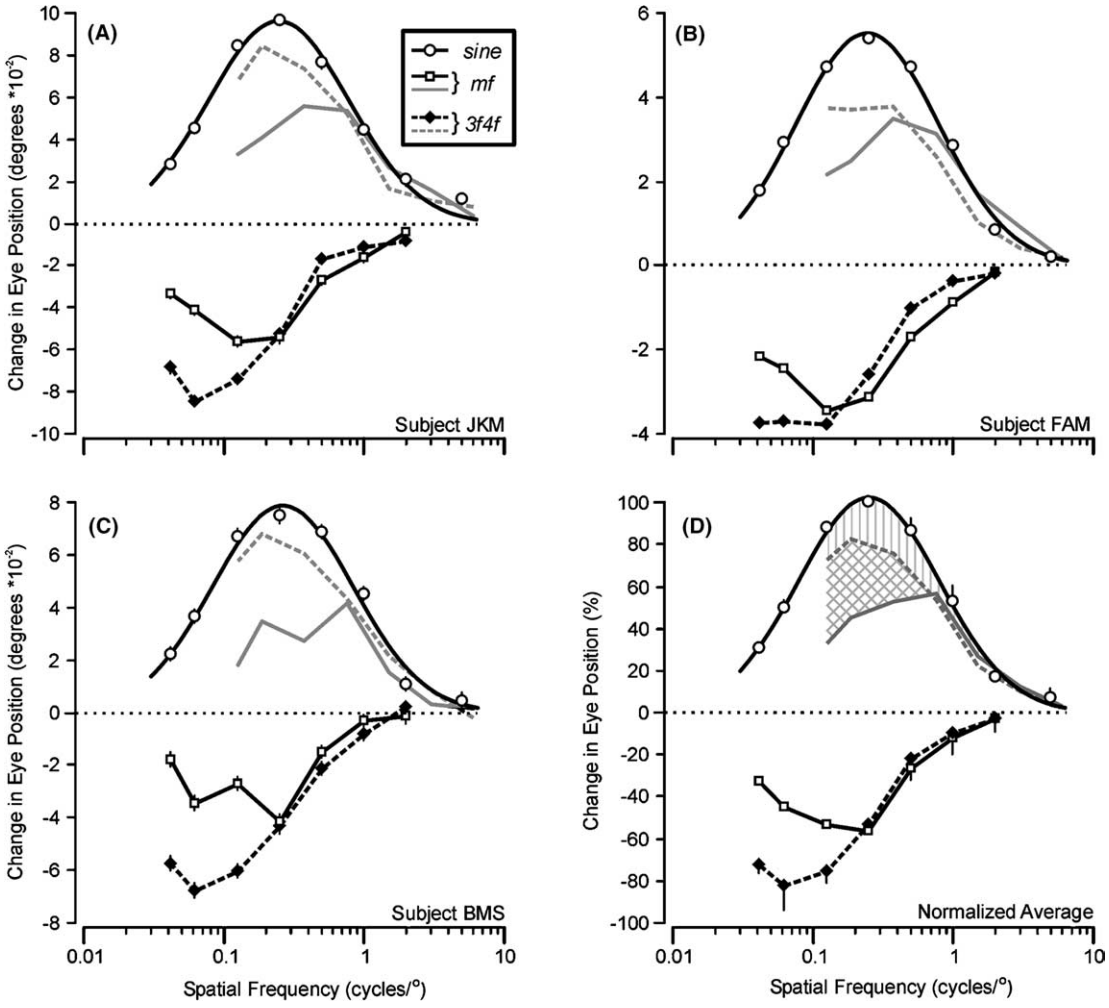

Fig. 3. The initial OFR: dependence on spatial frequency (R–L response measures). Plots show the horizontal OFR elicited by successive horizontal steps (each 1/4 of the fundamental wavelength) applied to *mf*, *3f4f* and pure sine-wave vertical gratings (3 subjects). The mean R–L response measures with pure sine wave stimuli (open circles) are always positive (OFR in the forward direction), whereas those with *mf* (open squares) and *3f4f* (filled diamonds) stimuli are always negative (OFR in the backward direction). Responses to *mf* and *3f4f* stimuli are also replotted as a function of the spatial frequency of their *3f* component with a sign inversion to permit easy comparison with the pure sine-wave data (*mf*, continuous gray line; *3f4f*, dashed gray line). The smooth black curves are best-fit Gaussian functions for the pure sine-wave data. A: subject JKM (171–195 trials per condition; SD's ranged 0.026–0.037°). B: subject FAM (186–196 trials per condition; SD's ranged 0.016–0.028°). C: subject BMS (92–146 trials per condition; SD's ranged 0.024–0.038°). D: Normalized averages for the 3 subjects (error bars, SD's). Contrast was 32% for the pure sinusoids and for the 3*f* components of the *mf* stimuli as well as for the *3f* and *4f* components of the *3f4f* stimuli.

the *mf* data were inverted and replotted as a function of the frequency of their 3*f* component, it was evident that their departure from the *3f4f* and sine-wave data generally occurred as the frequency of the 3*f* component dropped progressively below 1 cycle/°: see the gray continuous lines in Fig. 3 and the cross hatching in Fig. 3(D) (Note that the contrasts of the *3f4f* and *mf* stimuli were such that their 3*f* components had the same contrast as the pure sine-wave gratings: 32%.).

2.2.2. A control experiment concerning the 5th and 7th harmonics of the mf stimulus

It is clear from Fig. 3 that the OFR elicited by the *mf* stimuli often fell appreciably short of those elicited by pure sine-wave stimuli whose spatial frequency and contrast matched their 3rd harmonic when the latter was <1 cycle/°. We investigated the rôle of the 5th and 7th harmonics in this shortfall by recording the OFR elicited by *mf* stimuli lacking one or both of these harmonics—termed here, the *mf-5* and *mf-5&7* stimuli. Fig. 4 shows the dependence on spatial frequency of the mean normalized OFR (based on the R–L response measures) elicited by the *mf*, *mf-5*, *mf-5&7* and pure sine-wave stimuli for all 3 subjects. Note, that in order to facilitate easy comparison with the sine-wave data, the *mf*, *mf-5, and mf-5&7* data in Fig. 4 have been inverted and plotted as a function of the frequency of their 3rd harmonic, cf., Fig. 3. It is evident from Fig. 4 that

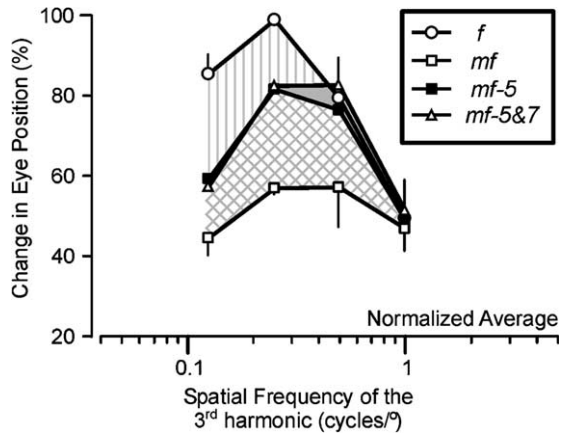

Fig. 4. Initial OFR to motion of *mf* stimuli: the rôle of the *5f* and *7f* harmonics (mean normalized R–L response measures for 3 subjects). Plot shows the dependence of the initial horizontal OFR elicited by successive horizontal steps (each 1/4 of the fundamental wavelength) applied to *mf*, *mf-5*, *mf-5&7* and pure sine-wave vertical gratings on the fundamental spatial frequency of those gratings. Responses to pure sine waves (open circles) were always positive, whereas those to *mf* (open squares), *mf-5* (filled squares) and *mf-5&7* (asterisks) gratings were always negative and are plotted as a function of the spatial frequency of their 3rd harmonic with a sign inversion to permit easy comparison with the pure sine-wave data. Contrast was 32% for the pure sinusoids and for the 3*f* components of the *mf*, *mf-5*, and *mf-5&7* stimuli. Error bars are SD's.

removing the 5th harmonic, which is the most prominent of the $4n + 1$ harmonics that shift 1/4 of their wavelength in the *for*ward direction, *increased* the amplitude of the OFR (in the *back*ward direction): see the cross hatching. Despite this, the *mf-5* data still fell short of the pure sine-wave data when the 3rd harmonic was <0.5 cycles/°. When we also removed the 7th harmonic, which—like the 3rd—is one of the $4n - 1$ harmonics that shift 1/4 of their wavelength in the *back*ward direction, there was little effect except for a seemingly anomalous *increase* in the amplitude of the OFR in the *back*ward direction when the spatial frequency of the 3rd harmonic was 0.5 cycles/°: see the triangular symbols in Fig. 4 (indicating the *mf-5&7* data).

2.2.3. A control experiment concerning coarse sampling of the mf stimulus

The minimum resolution of our display was 40 pixels/° and the *mf* stimuli were synthesized using only the odd harmonics below the Nyquist Frequency (20 cycles/°) in order to avoid spatial aliasing. However, this meant that the harmonics just below the Nyquist Frequency were coarsely sampled—being rendered by as few as 2 pixels/cycle. We did an additional control experiment in which we examined the effect of limiting the spatial frequency of the *mf* stimuli to 1/4 of the Nyquist Frequency (5 cycles/°), which meant that the highest spatial frequencies in these broadband stimuli would be rendered by at least 8 pixels/cycle.[2] To permit easy comparison, we also collected data using *mf* stimuli rendered up to the Nyquist Frequency, as in our original experiment. The R–L response measures for our 3 subjects indicated that restricting the harmonic content to 1/4 the Nyquist Frequency had little effect on the initial OFR. There were small differences between the two data sets for particular subjects that were sometimes statistically significant for particular spatial frequencies (paired *t*-test, $p < 0.05$), but there was no spatial frequency at which more than one of the three subjects showed significant differences. These data suggest that, in general, the coarsely sampled harmonics were not a significant factor in our experiments with the *mf* stimulus.

2.3. Discussion of Experiment 1 and associated controls

The initial OFR elicited by 1/4-wavelength steps applied to pure sine-wave stimuli were always in the forward direction and showed a band-pass dependence on log spatial frequency that was well fit by a Gaussian. The initial OFR elicited by 1/4-wavelength steps applied to *mf* stimuli were always in the backward direction, which was the direction of the principal Fourier component, the 3rd harmonic. In fact, when the spatial frequency of that 3rd harmonic was 1 cycle/° or more, the initial OFR elicited with the *mf* stimuli were very similar to those obtained with pure sinusoids whose spatial frequency and contrast matched the 3rd harmonic. However, when the spatial frequency of that 3rd harmonic was <1 cycle/°, the *mf* data fell short of the pure sine-wave data. Possible factors in this shortfall are the higher harmonics, distortion products and the motion of the features. The initial OFR elicited by 1/4-wavelength steps applied to *3f4f* stimuli were also always in the backward direction, which was the direction of the *3f* component, but again fell short of the OFR elicited by pure sine-wave stimuli whose spatial frequency and contrast matched that of the *3f* component, though generally by a smaller margin than the *mf* data. Again, the shortfall might have been due to higher harmonics—though this time there is only the *4f* component (whose images remained stationary)—as well as distortion products and the motion of the features. We will now address each of these three factors in turn.

2.3.1. Higher harmonics

The data obtained with the *mf-5* stimuli indicated that much—but not all—of this shortfall with the *mf* stimuli at low spatial frequencies was due to the influence of the next largest harmonic, the 5th, which is

[2] Note that the spatial frequency of the pure sine-wave stimuli used in this study never exceeded 5 cycles/°, and the spatial frequency of the 4*f* component of the *3f4f* stimulus was always <3 cycles/°.

one of the $4n + 1$ harmonics that shifts in the forward direction. That this 5th harmonic exerted little influence when the 3rd harmonic was 1 cycle/° (or more) is perhaps a little surprising: when the spatial frequency of the 3rd harmonic was 1 cycle/°, the 5th harmonic had a spatial frequency of 1.67 cycles/°, which is well below the high-frequency cutoff for OFR (>5 cycles/°) and its contrast (almost 20%) should have been sufficient to generate significant OFR (as we will see in the next section). That the 5th harmonic of the *mf* stimulus exerted greater influence when the frequency of the 3rd harmonic fell below 1 cycle/° might be expected because its efficacy would increase steadily as its spatial frequency fell from 1.67 cycles/°: the peak of the pure sinusoid data in Fig. 3 is 0.25 cycles/° and the 5th harmonic of the *mf* stimulus reached this spatial frequency when the 3rd harmonic was 0.15 cycles/°, which is only just above the low-frequency limit for the *mf* data shown in Fig. 3.

Interestingly, removing the 7th harmonic from the *mf-5* stimuli generally had little impact except for *increasing* the OFR slightly in the *back*ward direction when the 3rd harmonic was 0.5 cycles/° (Fig. 4) even though the 7th harmonic is one of the $n - 1$ harmonics that shift in the *back*ward direction. One possible factor here is that the apparent speed of the 7th harmonic is only ~43% of the apparent speed of the 3rd harmonic: if the overall drive to OFR results from some sort of average-speed signal then the 7th harmonic might actually work to reduce OFR below the level called for by the (faster) 3rd harmonic, hence its exclusion would increase OFR. This would be consistent with the speed-averaging described by Watamaniuk and Duchon (1992). On the other hand, the total insensitivity to removal of the 7th harmonic at the lower spatial frequencies is puzzling, given that the contrast of that component was almost 14% and, at the lower limit of the spatial-frequency range shown in Fig. 4, for example, its spatial frequency (0.29 cycles/°) would have been close to the optimal for OFR (0.25 cycles/°).

That the data obtained with the *3f4f* stimuli also fell short of the pure sine-wave data might have been due, at least in part, to the stationary *4f* component, though a pure energy-based mechanism would be relatively immune to the presence of such a stationary pedestal. For discussion of this point see Lu and Sperling (1995, 1996, 2001).

2.3.2. Distortion products

There is substantial evidence for compressive nonlinearities early in the visual pathway (e.g., He & Macleod, 1998; MacLeod & He, 1993; MacLeod, Williams, & Makous, 1992) and these result in distortion products that might have been visible to the energy-based mechanisms mediating OFR in our experiments. However, the exact form of these distortion products with our complex stimuli is not clear so we examined this issue using a non-linear filter, based on a variant of the Naka–Rushton equation (Naka & Rushton, 1966) used by Scott-Samuel and Georgeson (1999), whose transfer function, $R(x)$, is given by the expression,

$$R_{\max}\frac{I(x)^n}{I(x)^n + S^n}, \tag{1}$$

where $R_{\max}$ is the maximum value of R (when I is large), $I(x)$ is the normalized luminance (i.e., expressed as a fraction of the mean luminance), exponent n is a constant, and S is the semi-saturation constant (value of $I(x)$ at which $R(x)$ has half its maximum value). The value of n was fixed at 1 so that the degree of compression was determined entirely by S: the lower its value, the greater the compression. Scott-Samuel and Georgeson (1999) surveyed previous studies (on the perceived location of blurred luminance edges) that had used compressive filters like this and they determined that the values of S obtained in those studies ranged from 0.5 to 3.5 with a clear tendency to increase with stimulus duration. We used a value of 0.5 for S, which was the value of obtained by Georgeson and Freeman (1997) whose stimuli had a duration (216 ms) that was the closest to ours. The value of $R_{\max}$ is not important here and, like Scott-Samuel and Georgeson (1999), we set its value to $2 + S$ so that the input and output ranged from zero to 2. The resulting filter was applied to the *mf, mf-5,* and *3f4f* luminance profiles and these were then analyzed with a fast Fourier transform (FFT).

This analysis indicated that the major distortion products with the *mf* stimulus were mostly even harmonics—the 2nd, 4th, 6th et seq. Effects on the odd harmonics were minor. When the *mf* stimulus shifts 1/4 of the wavelength of its fundamental, the *i*th even harmonic shifts *i*/4 multiples of its wavelength, with the net result that the 2nd, 6th, 10th etc., harmonics shift 1/2 of their wavelength and so are seen as stationary and flickering, whereas the 4th, 8th, 12th etc., harmonics shift one complete wavelength and hence are seen as stationary and unmodulated. Thus, the major distortion products are all stationary, and half of them—including the most prominent one, the 2nd harmonic, with a contrast up to 35% of that of the 3rd harmonic in our simulation—undergo counterphase flicker. These stationary images (especially the flickering ones?) might well interfere with the motion detectors mediating OFR, resulting in a net attenuation of OFR, though, as mentioned above, a pure energy-based mechanism would be blind to the stationary harmonics (Lu & Sperling, 1995, 1996, 2001). In general, removing the 5th harmonic (as in the *mf-5* stimulus) reduced these even harmonics and removing the 7th harmonic (as in the *mf-5&7* stimulus) slightly reinforced this effect, suggesting that the distortion products associated with these stimuli might have had a slightly less attenuating effect on OFR than

those associated with the *mf* stimuli. In sum, this analysis opens up the possibility that Fourier components secondary to early compressive non-linearities (distortion products) undermined the OFR elicited by the primary Fourier components of the various *mf* stimuli.[3] That the difference between the data obtained with the various *mf* stimuli and the pure sine-waves (matching the 3rd harmonics) was greatest at the lower spatial frequencies (Fig. 3) might in part reflect the fact that the higher-frequency distortion products would have greater efficacy when the *mf* stimuli were of lower spatial frequency.

The distortion products associated with the *3f4f* stimuli consisted mainly of the 1st and 7th odd harmonics, which have opposing influences on OFR, and the 6th and 8th harmonics, both of which are stationary and so might work to attenuate OFR.

In sum, our analysis of the distortion products associated with our various grating patterns indicates that they might well be responsible for attenuating the OFR at lower spatial frequencies. Unfortunately, the exact extent of this attenuation is unclear.

2.3.3. Feature-based mechanism—third-order motion?

Feature-based mechanisms made at best a very minor contribution to the OFR associated with our complex grating patterns when the spatial frequency of the 3*f* component exceeded 1 cycle/°. The situation was less clear for complex gratings of lower spatial frequency, which generated OFR that fell short of those to the matched pure sine waves, though the clear implication of the previous discussion is that the shortfall here might well have resulted in large part from higher harmonics and distortion products.

Lu and Sperling (2002) have recently challenged the idea that the missing fundamental paradigm can be used to dissociate energy-based and feature-based mechanisms. These workers have argued that there are three separate motion systems, rather than two, and have hypothesized a third-order mechanism that first computes a salience map using "important" landmarks and then applies a motion-energy algorithm. Lu and Sperling concluded that the peaks and troughs in the *mf* stimulus constitute a salience map that shows space-time modulations very similar to those of the 3rd harmonic. This led them to suggest that the missing fundamental "paradigm may fail to distinguish between a third-order motion (or feature-tracking) computation and a motion-energy computation". However, two defining characteristics of this third-order mechanism—sluggish dynamics and strong dependence on attention (Lu & Sperling, 2001)—strongly suggest that it cannot have mediated the OFR under discussion here: (1) initial human OFR to sine-wave gratings have band-pass temporal-frequency characteristics with a peak at 16 Hz (Gellman et al., 1990) whereas the temporal-frequency-tuning function for third-order stimuli is low-pass and already attenuated 3 dB at ~3 Hz (Lu & Sperling, 2001); (2) we have preliminary evidence that the earliest OFR under consideration here are not modulated by attention, though later components clearly are (Sheliga & Miles, unpublished observations).

[3] Note that the distortion products associated with the pure *3f* stimulus were simple multiples (*6f*, *9f* etc.) with progressively decreasing amplitude, so that the most powerful one (*6f*) was the only one with significant contrast in our analysis (~3.3%).

3. Experiment 2: Dependence of OFR on contrast

The clear indication from Experiment 1 was that the OFR elicited by 1/4-wavelength steps applied to the *mf*, *mf-5* and *3f4f* stimuli were strongly dependent on the principal Fourier component. In the present experiment we examined these responses further by investigating their dependence on contrast and were especially interested in comparing the OFR elicited by the *mf* and *3f4f* stimuli with those elicited when identical steps were applied to pure sine-wave gratings with spatial frequencies that matched those of the 1*f* and 3*f* components.

3.1. Methods

The subjects, as well as most of the methods and procedures, were identical to those used in Experiment 1, and only those that were different will be described here.

3.1.1. Visual display

The fundamental spatial frequencies of the *mf* and the *3f4f* stimuli were fixed at 0.153 cycles/° (wavelength, 6.55°, which was 264 pixels), while the pure sine-wave gratings had two spatial frequencies: 0.153 cycles/° ("the *1f* stimulus") and 0.458 cycles/° (wavelength, 2.183°, which was 88 pixels: "the *3f* stimulus"). Experiment 1 had indicated that pure sine-wave stimuli with the spatial frequencies of these *1f* and *3f* stimuli elicit robust OFR of similar amplitude. This was an important consideration in an experiment concerned with complex grating stimuli and the relative efficacy of their features, which repeat with the frequency of the fundamental, and of their principal Fourier component, which is the 3rd harmonic. The successive phase shifts used to generate the apparent motion always had the same absolute amplitude, 1.65° (66 pixels), which was 1/4 of the fundamental wavelength of the *mf*, *3f4f* and *1f* stimuli and 3/4 of the wavelength of the *3f* stimulus. The dependent variable was the Michelson contrast, randomly sampled each trial from a lookup table. The contrast values in the lookup table for the *1f* and *3f* stimuli were 0.5%, 1%, 2%, 4%, 8%, 16%, 32%, and 64%. The contrasts

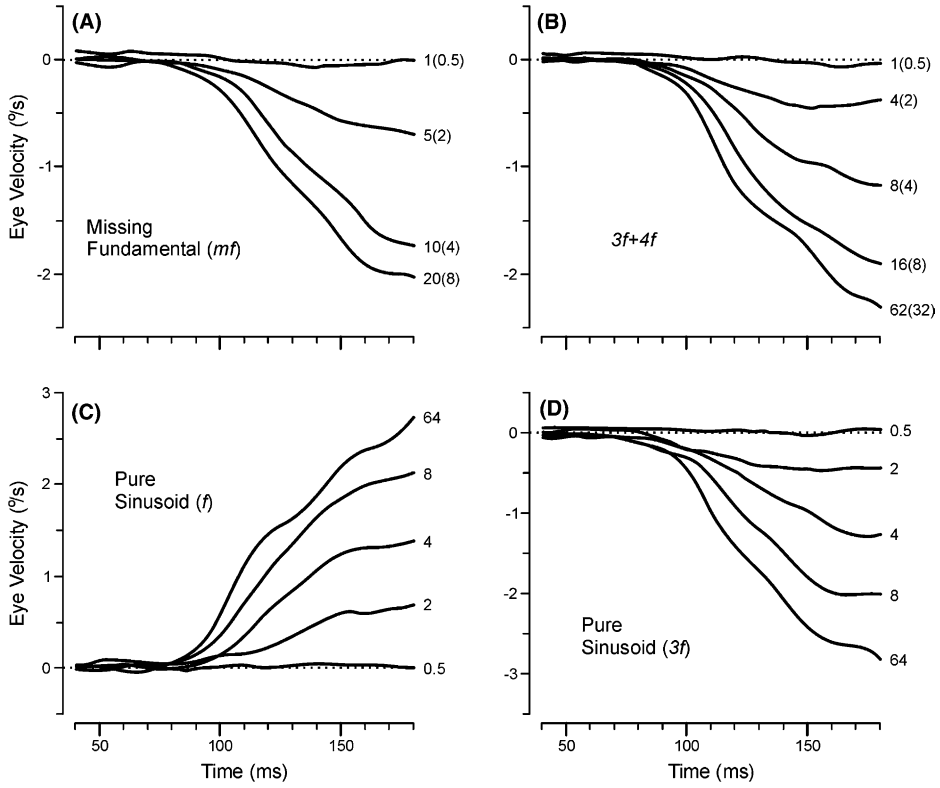

Fig. 5. The initial OFR: dependence on contrast (R–L eye velocity traces). Traces show the horizontal OFR elicited when successive steps (each 1.65°) were applied to various types of vertical grating pattern (subject, JKM). A: *mf* stimulus (spatial frequency, 0.153 cycles/°). B: *3f4f* stimulus (spatial frequency, 0.153 cycles/°). C: pure sine-wave stimulus with spatial frequency equal to that of the fundamental of the *mf* and *3f4f* stimuli (''the *1f* stimulus'', spatial frequency, 0.153 cycles/°). D: a pure sine-wave stimulus with spatial frequency equal to that of the 3rd harmonic of the *mf* and *3f4f* stimuli (''the *3f* stimulus'', spatial frequency, 0.458 cycles/°). Each trace is the mean difference in eye velocity to rightward and leftward motion (R–L) for 193–225 repetitions of the stimulus. The dotted lines indicate zero eye velocity. Note that time on the abscissa starts 40 ms after the occurrence of the first step. The numbers at the ends of the traces indicate the contrasts of the whole pattern (no parentheses) and its 3*f* component (in parentheses).

of the *mf* and *3f4f* stimuli were selected so that the contrasts of their *3f* components matched the contrasts of the 3*f* stimuli (up to a maximum of 32%). The *mf* stimuli were synthesized up to the Nyquist Frequency, so that the highest harmonic was the 131st (20 cycles/°) with a contrast of 0.74%, which we estimate is close to—or even below—the threshold for OFR (see later discussion).

3.1.2. Procedures

These were as in Experiment 1 except that each block of trials had 60 randomly interleaved stimulus combinations: 4 grating patterns, each with 7 or 8 contrasts (indicated above) and 2 directions of motion.

3.2. Results

The initial OFR elicited by 1/4-wavelength steps applied to *mf* and *3f4f* stimuli were again always in the direction of the 3rd harmonic, this time over the full range of contrasts to which the subjects were responsive. Sample mean eye velocity profiles from one subject are shown in Fig. 5 and this time we show the directional differences (mean OFR to rightward shifts minus mean OFR to leftward shifts) so that *up*ward deflections of the traces in Fig. 5 are in the *forward* direction. Clearly, all responses to the *mf* and *3f4f* stimuli were in the *back*ward direction: see the *down*ward deflections in Fig. 5(A) and (B). Note that the two numbers at the ends of the traces indicate the contrasts of the patterns and of their 3*f* components (the latter is in parentheses). The direction of the OFR elicited when steps were applied to the pure sine-wave stimuli were exactly as expected: all steps had the same absolute amplitude, which was 1/4 of the fundamental wavelength of the *1f* stimuli, so that the OFR were in the forward direction with the *1f* stimuli (upward deflections in Fig. 5(C)) and in the backward direction with the *3f* stimuli (downward deflections in Fig. 5(D)).

The quantitative dependence on contrast, based on the mean R–L response measures, was quite similar in all subjects: see the plots in Fig. 6. With the *1f* and *3f* stimuli (closed and open circles, respectively, in Fig. 6), the OFR for each of the 3 subjects showed a

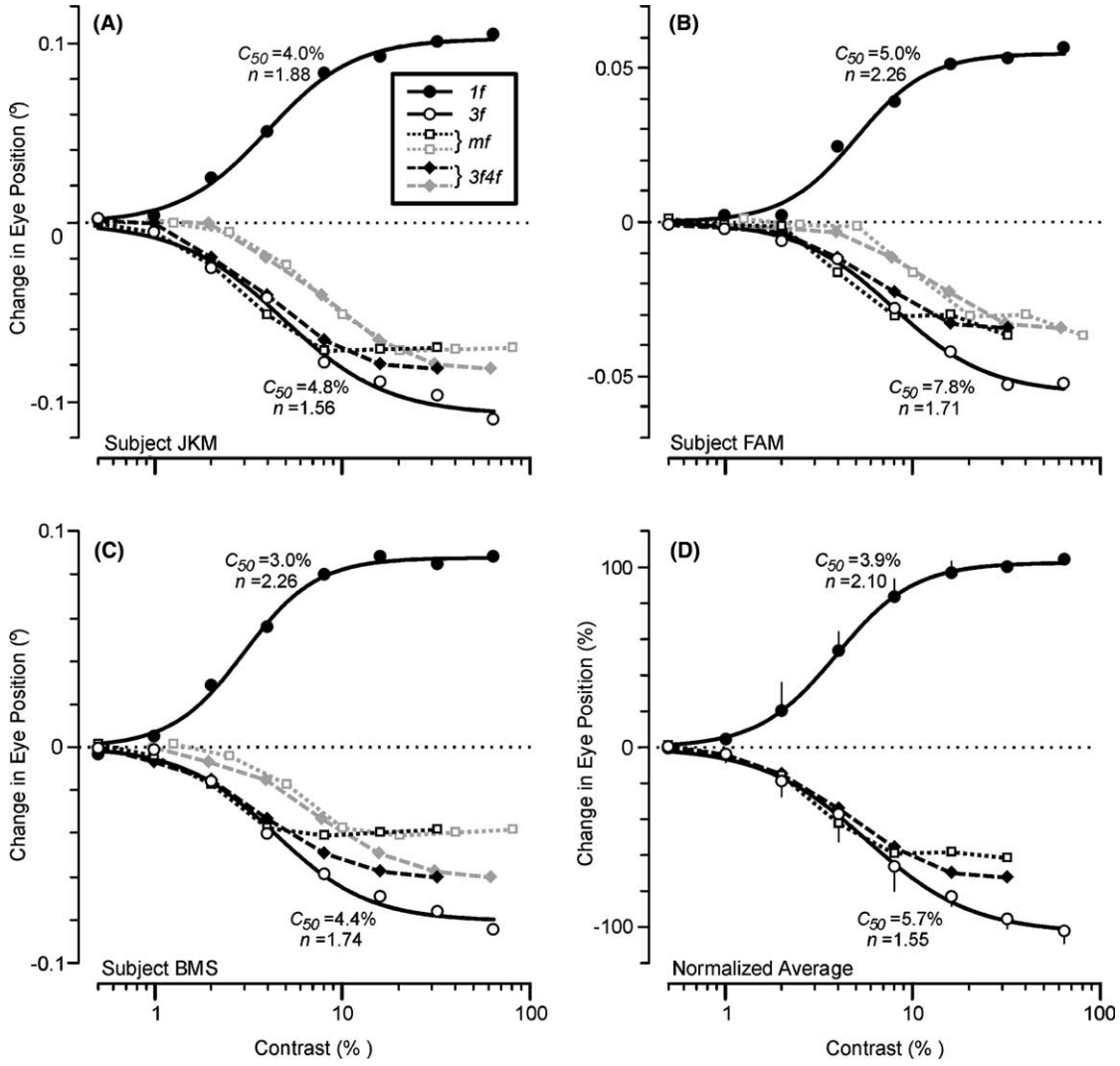

Fig. 6. The initial OFR: dependence on contrast (R–L response measures). Plots show the horizontal OFR elicited when successive steps (each 1.65°) were applied to *mf* and *3f4f* gratings as well as to pure sine-wave gratings whose spatial frequencies matched the 1*f* or 3*f* components of the complex gratings, exactly as in Fig. 5 (3 subjects). Responses to the pure *1f* sine waves (filled circles) were always positive (OFR in the forward direction), whereas those to *mf* (gray open squares, gray dotted lines), *3f4f* (gray filled diamonds, gray dashed lines), and the pure *3f* sine waves (open circles) gratings were always negative (OFR in the backward direction). Responses to the *mf* and *3f4f* gratings are also replotted as a function of the contrast of their 3*f* component to permit easy comparison with the pure *3f* sine-wave data (*mf*, black open squares and dotted line; *3f4f*, black filled diamonds and dashed line). The smooth black curves are best-fit Naka–Rushton functions for the pure sine-wave data and the values of their c_{50} and n parameters are shown nearby. A: subject JKM (193–225 trials per condition; SD's ranged 0.025–0.036°). B: subject FAM (221–246 trials per condition; SD's ranged 0.016–0.024°). C: subject BMS (164–177 trials per condition; SD's ranged 0.019–0.031°). D: Normalized averages for the 3 subjects (error bars are SD's). Spatial frequencies were as given in Fig. 5.

monotonic rise from a threshold contrast of ~1% (Fig. 6(A)–(C)) and, together with the mean normalized data for all 3 subjects (Fig. 6(D)), were fitted with the following expression:

$$R_{\max}\frac{c^n}{c^n + c_{50}^n}, \qquad (2)$$

where $R_{\max}$ is the maximum attainable response, c is the contrast, c_{50} is the semi-saturation contrast (at which the response has half its maximum value), and n is the exponent that sets the steepness of the curves. This expression (like expression 1) is based on the Naka–Rushton equation (Naka & Rushton, 1966) and various studies have shown that it provides a good fit to the contrast dependence curves of neurons in the LGN, V1 and MT of monkeys (e.g., Albrecht, Geisler, Frazor, & Crane, 2002; Albrecht & Hamilton, 1982; Heuer & Britten, 2002; Sclar, Maunsell, & Lennie, 1990), as well as to the human contrast dependence curves for the OFR to moving sine-wave gratings and unikinetic plaid patterns (Masson & Castet, 2002). The continuous smooth curves in Fig. 6 are the best fit curves using expression 2 and are excellent approximations to the data with r^2 values of 0.99 or greater in all cases. The parameters,

c_{50} and n, for these various fits are printed beside the curves in Fig. 6. The best-fit curves for the *3f* data are always slightly less steep than those for the *1f* data (n for the normalized averages of the 3 subjects shown in Fig. 6(D): 1.55 and 2.10, respectively), and the *3f* data always reach 50% maximum at a contrast that is a little higher than for the *1f* data (c_{50} for the normalized averages in Fig. 6(D): 5.7% and 3.9%, respectively). The contrast response data for the *3f4f* stimuli (gray filled diamonds and gray dashed lines in Fig. 6) and for the *mf* stimuli (gray open squares and gray dotted lines in Fig. 6) lie to the right of the data obtained with the *3f* stimuli, which again is perhaps not surprising if the response is driven mainly by the motion of the 3*f* component rather than the motion of the overall pattern. If the responses to the *3f4f* and *mf* gratings were solely determined by their 3*f* component then, when replotted as a function of the contrast of this component, the *3f4f* and *mf* data should show the same dependence on contrast as the *3f* sine-wave data. When so replotted the *3f4f* and *mf* data do closely follow the data obtained with the *3f* stimuli at low contrasts, but gradually fall increasingly short as contrast exceeds 4–8%: see the black diamonds and black squares in Fig. 6.

3.3. Discussion of experiment 2

The initial OFR elicited by the *mf* and *3f4f* stimuli were always in the direction of the principal Fourier (3*f*) component and, when plotted in terms of the contrast of their 3rd harmonic, their amplitudes generally matched those obtained with the *3f* stimuli for contrasts up to 4–8% but fell progressively short with higher contrasts (Fig. 6). As discussed earlier, this shortfall is at least in part due to the higher harmonics but it might also reflect the influence of distortion products and/or a feature-based mechanism. Importantly, Scott-Samuel and Georgeson (1999) used a nulling technique to show that the distortion products associated with second-order motion stimuli (defined by a contrast-modulated carrier) increased as the square of the contrast, exactly as predicted by the compressive non-linearity that they (and we) used to model distortion products (see Section 2.3.2). This might be one reason why the *mf* and *3f4f* data fell increasingly short of the pure *3f* data as contrast increased. However, there is evidence from the experiments of Masson and Castet (2002) that any contribution from a feature- or pattern-based mechanism might also be seen only at higher contrasts. These workers showed that motion applied to only one of two sine-wave gratings making up a plaid (the so-called unikinetic plaid) elicited OFR with two components: initially, the response was in the direction of the moving grating—referred to as the *component* (first-order?) motion—and then, after ~20 ms, the response began to acquire an orthogonal component—in the direction of the *pattern* (second-order?) motion. Masson and Castet examined the dependence of the initial OFR on the contrast of the stationary sine wave and then fitted the Naka–Rushton equation to their response measures: on average, the value of the c_{50} parameter for the pattern response was 5 times greater than that for the component response (to pure sine waves), whereas the value of the n parameter was quite similar in the two cases.[4] This indicates that, at low contrast, the contrast response curves for OFR were much flatter when the motion was applied to the pattern than when it was applied to pure sine waves. This is apparent in Fig. 14 of Masson and Castet's paper, which shows contrast-dependency curves for two subjects and clearly indicates that OFR to the pattern motion were not significant until the contrast exceeded 10%. Such a pattern-based contribution might help to explain why in our experiments the *mf* and *3f4f* data fell short of the pure *3f* data only at higher contrasts, i.e., >8%.

4. Closing remarks

Our experiments with complex grating patterns indicate that the earliest OFR are strongly dependent on the motion of the principal Fourier component, especially at high spatial frequency ($\geqslant$1 cycle/°) and low contrast ($\leqslant$8%). This is consistent with a previous suggestion—based on the finding that initial OFR are reversed with first-order reversed-phi stimuli (Masson et al., 2002a)—that initial OFR are mediated by oriented spatio-temporal visual filters as in the well-known energy model of motion detection. The possibility exists that a feature-based mechanism contributed to our data at lower spatial frequencies and higher contrasts but our analyses indicate that higher harmonics and distortion products were also likely contributors here, reducing the likelihood that a feature-based mechanism had more than a very minor rôle. Indeed, we suggest that initial OFR provide a model system for studying the neural mechanisms sensing first-order motion energy, objectively and quantitatively.

References

Adelson, E. H. (1982). Some new motion illusions, and some old ones, analysed in terms of their Fourier components. *Investigative Ophthalmology and Visual Science, 34*(Suppl.), 144 [Abstract].

[4] However, for the contrast dependence in this study, the Michelson contrast was held constant (at 100%) so increases in the contrast of the static grating were offset by equivalent decreases in the contrast of the moving grating.

Adelson, E. H., & Bergen, J. R. (1985). Spatiotemporal energy models for the perception of motion. *Journal of the Optical Society of America A, 2*, 284–299.

Albrecht, D. G., Geisler, W. S., Frazor, R. A., & Crane, A. M. (2002). Visual cortex neurons of monkeys and cats: temporal dynamics of the contrast response function. *Journal of Neurophysiology, 88*, 888–913.

Albrecht, D. G., & Hamilton, D. B. (1982). Striate cortex of monkey and cat: contrast response function. *Journal of Neurophysiology, 48*, 217–237.

Archer, S. M., Miller, K. K., & Helveston, E. M. (1987). Stereoscopic contours and optokinetic nystagmus in normal and stereoblind subjects. *Vision Research, 27*, 841–844.

Baro, J. A., & Levinson, E. (1988). Apparent motion can be perceived between patterns with dissimilar spatial frequencies. *Vision Research, 28*, 1311–1313.

Benson, P. J., & Guo, K. (1999). Stages in motion processing revealed by the ocular following response. *Neuroreport, 10*, 3803–3807.

Braddick, O. (1974). A short-range process in apparent motion. *Vision Research, 14*, 519–527.

Brainard, D. H. (1997). The Psychophysics Toolbox. *Spatial Vision, 10*, 433–436.

Brown, R. O., & He, S. (2000). Visual motion of missing-fundamental patterns: motion energy versus feature correspondence. *Vision Research, 40*, 2135–2147.

Butzer, F., Ilg, U. J., & Zanker, J. M. (1997). Smooth-pursuit eye movements elicited by first-order and second-order motion. *Experimental Brain Research, 115*, 61–70.

Cavanagh, P. (1992). Attention-based motion perception. *Science, 257*, 1563–1565.

Cavanagh, P., & Mather, G. (1989). Motion: the long and short of it. *Spatial Vision, 4*, 103–129.

Chubb, C., & Sperling, G. (1988). Drift-balanced random stimuli: a general basis for studying non-Fourier motion perception. *Journal of the Optical Society of America A, 5*, 1986–2007.

Collewijn, H., Van Der Mark, F., & Jansen, T. C. (1975). Precise recording of human eye movements. *Vision Research, 15*, 447–450.

Derrington, A. M., Allen, H. A., & Delicato, L. S. (2004). Visual mechanisms of motion analysis and motion perception. *Annual Review of Psychology, 55*, 181–205.

Fox, R., Lehmkuhle, S., & Leguire, L. E. (1978). Stereoscopic contours induce optokinetic nystagmus. *Vision Research, 18*, 1189–1192.

Fuchs, A. F., Reiner, D., & Pong, M. (1996). Transfer of gain changes from targeting to other types of saccade in the monkey: constraints on possible sites of saccadic gain adaptation. *Journal of Neurophysiology, 76*, 2522–2535.

Gellman, R. S., Carl, J. R., & Miles, F. A. (1990). Short latency ocular-following responses in man. *Visual Neuroscience, 5*, 107–122.

Georgeson, M. A., & Freeman, T. C. (1997). Perceived location of bars and edges in one-dimensional images: computational models and human vision. *Vision Research, 37*, 127–142.

Georgeson, M. A., & Harris, M. G. (1990). The temporal range of motion sensing and motion perception. *Vision Research, 30*, 615–619.

Georgeson, M. A., & Shackleton, T. M. (1989). Monocular motion sensing, binocular motion perception. *Vision Research, 29*, 1511–1523.

Grzywacz, N. M., Watamaniuk, S. N., & McKee, S. P. (1995). Temporal coherence theory for the detection and measurement of visual motion. *Vision Research, 35*, 3183–3203.

Hammett, S. T., Ledgeway, T., & Smith, A. T. (1993). Transparent motion from feature- and luminance-based processes. *Vision Research, 33*, 1119–1122.

Harris, L. R., & Smith, A. T. (1992). Motion defined exclusively by second-order characteristics does not evoke optokinetic nystagmus. *Visual Neuroscience, 9*, 565–570.

Harris, L. R., & Smith, A. T. (2000). Interactions between first- and second-order motion revealed by optokinetic nystagmus. *Experimental Brain Research, 130*, 67–72.

Hawken, M. J., & Gegenfurtner, K. R. (2001). Pursuit eye movements to second-order motion targets. *Journal of the Optical Society of America A, 18*, 2282–2296.

Hays, A. V., Richmond, B. J., & Optican, L. M. (1982). A UNIX-based multiple process system for real-time data acquisition and control. In *WESCON Conference Proceedings, Vol. 2* (pp. 1–10).

He, S., & Macleod, D. I. (1998). Contrast-modulation flicker: dynamics and spatial resolution of the light adaptation process. *Vision Research, 38*, 985–1000.

Heuer, H. W., & Britten, K. H. (2002). Contrast dependence of response normalization in area MT of the rhesus macaque. *Journal of Neurophysiology, 88*, 3398–3408.

Johnston, A., & Clifford, C. W. (1995). Perceived motion of contrast-modulated gratings: predictions of the multi-channel gradient model and the role of full-wave rectification. *Vision Research, 35*, 1771–1783.

Johnston, A., McOwan, P. W., & Buxton, H. (1992). A computational model of the analysis of some first-order and second-order motion patterns by simple and complex cells. *Proceedings of the Royal Society, B, Biological Sciences, 250*, 297–306.

Krauzlis, R. J. (2004). Recasting the smooth pursuit eye movement system. *Journal of Neurophysiology, 91*, 591–603.

Lindner, A., & Ilg, U. J. (2000). Initiation of smooth-pursuit eye movements to first-order and second-order motion stimuli. *Experimental Brain Research, 133*, 450–456.

Lu, Z. L., & Sperling, G. (1995). The functional architecture of human visual motion perception. *Vision Research, 35*, 2697–2722.

Lu, Z. L., & Sperling, G. (1996). Three systems for visual motion perception. *Current Directions in Psychological Science, 5*, 44–53.

Lu, Z. L., & Sperling, G. (2001). Three-systems theory of human visual motion perception: review and update. *Journal of the Optical Society of America A, 18*, 2331–2370.

Lu, Z. L., & Sperling, G. (2002). Stereomotion is processed by the third-order motion system: reply to comment on three-systems theory of human visual motion perception: review and update. *Journal of the Optical Society of America A, 19*, 2144–2153.

MacLeod, D. I., & He, S. (1993). Visible flicker from invisible patterns. *Nature, 361*, 256–258.

MacLeod, D. I., Williams, D. R., & Makous, W. (1992). A visual nonlinearity fed by single cones. *Vision Research, 32*, 347–363.

Masson, G. S., Busettini, C., Yang, D.-S., & Miles, F. A. (2001). Short-latency ocular following in humans: sensitivity to binocular disparity. *Vision Research, 41*, 3371–3387.

Masson, G. S., & Castet, E. (2002). Parallel motion processing for the initiation of short-latency ocular following in humans. *The Journal of Neuroscience, 22*, 5149–5163.

Masson, G. S., Yang, D. S., & Miles, F. A. (2002a). Reversed short-latency ocular following. *Vision Research, 42*, 2081–2087.

Masson, G. S., Yang, D. S., & Miles, F. A. (2002b). Version and vergence eye movements in humans: open-loop dynamics determined by monocular rather than binocular image speed. *Vision Research, 42*, 2853–2867.

Miles, F. A., Kawano, K., & Optican, L. M. (1986). Short-latency ocular following responses of monkey. I. Dependence on temporospatial properties of visual input. *Journal of Neurophysiology, 56*, 1321–1354.

Naka, K. I., & Rushton, W. A. (1966). S-potentials from colour units in the retina of fish (Cyprinidae). *Journal of Physiology, 185*, 536–555.

Nishida, S., Ledgeway, T., & Edwards, M. (1997). Dual multiple-scale processing for motion in the human visual system. *Vision Research, 37*, 2685–2698.

Pelli, D. G. (1997). The VideoToolbox software for visual psychophysics: transforming numbers into movies. *Spatial Vision, 10*, 437–442.

Pelli, D. G., & Zhang, L. (1991). Accurate control of contrast on microcomputer displays. *Vision Research, 31*, 1337–1350.

Ramachandran, V. S., & Cavanagh, P. (1987). Motion capture anisotropy. *Vision Research, 27*, 97–106.

Read, J. C., & Cumming, B. G. (2003). Testing quantitative models of binocular disparity selectivity in primary visual cortex. *Journal of Neurophysiology, 90*, 2795–2817.

Reichardt, W. (1961). Autocorrelation, a principle for evaluation of sensory information by the central nervous system. In W. A. Rosenblith (Ed.), *Sensory communication* (pp. 303–317). Cambridge, MA: MIT Press.

Robinson, D. A. (1963). A method of measuring eye movement using a scleral search coil in a magnetic field. *Institute of Electronic and Electrical Engineers: Transactions in Biomedical Engineering, BME-10*, 137–145.

Sclar, G., Maunsell, J. H., & Lennie, P. (1990). Coding of image contrast in central visual pathways of the macaque monkey. *Vision Research, 30*, 1–10.

Scott-Samuel, N. E., & Georgeson, M. A. (1999). Does early non-linearity account for second-order motion? *Vision Research, 39*, 2853–2865.

Smith, A. T. (1994). Correspondence-based and energy-based detection of second-order motion in human vision. *Journal of the Optical Society of America A, 11*, 1940–1948.

Taub, E., Victor, J. D., & Conte, M. M. (1997). Nonlinear preprocessing in short-range motion. *Vision Research, 37*, 1459–1477.

Usui, S., & Amidror, I. (1982). Digital low-pass differentiation for biological signal processing. *IEEE Transactions on Biomedical Engineering, 29*, 686–693.

Vaina, L. M., & Cowey, A. (1996). Impairment of the perception of second order motion but not first order motion in a patient with unilateral focal brain damage. *Proceedings of the Royal Society, B, Biological Sciences, 263*, 1225–1232.

Vaina, L. M., Cowey, A., & Kennedy, D. (1999). Perception of first- and second-order motion: separable neurological mechanisms? *Human Brain Mapping, 7*, 67–77.

Vaina, L. M., Makris, N., Kennedy, D., & Cowey, A. (1998). The selective impairment of the perception of first-order motion by unilateral cortical brain damage. *Visual Neuroscience, 15*, 333–348.

Vaina, L. M., & Soloviev, S. (2004). First-order and second-order motion: neurological evidence for neuroanatomically distinct systems. *Progress in Brain Research, 144*, 197–212.

van Santen, J. P., & Sperling, G. (1985). Elaborated Reichardt detectors. *Journal of the Optical Society of America A, 2*, 300–321.

Watamaniuk, S. N., & Duchon, A. (1992). The human visual system averages speed information. *Vision Research, 32*, 931–941.

Yang, D. S., FitzGibbon, E. J., & Miles, F. A. (2003). Short-latency disparity-vergence eye movements in humans: sensitivity to simulated orthogonal tropias. *Vision Research, 43*, 431–443.

Yang, D. S., & Miles, F. A. (2003). Short-latency ocular following in humans is dependent on absolute (rather than relative) binocular disparity. *Vision Research, 43*, 1387–1396.